Journal of The Electrochemical Society

Electrodeposited Bimetallic (PtPd, PtRu, PtSn) Catalysts on Titanium Support for Methanol Oxidation in Direct Methanol Fuel Cells

Journal of The Electrochemical Society, 2020 **167** 024512

Electrodeposited Bimetallic (PtPd, PtRu, PtSn) Catalysts on Titanium Support for Methanol Oxidation in Direct Methanol Fuel Cells

Bincy George Abraham, Rashmi Bhaskaran, and Raghuram Chetty[*,z]

Department of Chemical Engineering, Indian Institute of Technology Madras, Chennai, India

The electrodeposition of platinum-based catalysts (PtPd, PtRu, and PtSn) using the pulse current deposition technique was carried out on titanium substrate to prepare electrodes of different compositions to identify a possible catalyst offering high catalytic activity towards methanol oxidation (MOR). Characterization by XRD, SEM, and EDX confirmed the deposition of catalysts with the desired composition with various morphologies of dendritic, spherical, and irregular deposits for PtPd, PtRu, and PtSn, respectively. Among the various compositions and binary metals studied, electrochemical results indicate PtRu/Ti with Pt to Ru ratio of 1:1 ($Pt_{50}Ru_{50}$/Ti) to be most active with lower onset potentials for CO oxidation (0.381 V) and methanol oxidation (0.545 V) along with higher peak current density of ~90 mA cm^{-2} compared to Pt/Ti (with onset potentials of 0.601 V for CO oxidation, 0.659 V for methanol oxidation and ~68 mA cm^{-2} peak current density). Moreover, the MOR catalytic activity retention after 1000 accelerated durability test cycles was the highest for $Pt_{50}Ru_{50}$/Ti at 55% compared to Pt/Ti and commercial Pt/C.

 [DOI: 10.1149/1945-7111/ab6a7d]

Manuscript submitted August 13, 2019; revised manuscript received November 25, 2019. Published January 28, 2020.

Supplementary material for this article is available online

Direct methanol fuel cells (DMFCs) have attracted considerable research attention for portable applications among the low-temperature fuel cells because of their easy fuel handling and enhanced storage safety in comparison to hydrogen.[1,2] However, several challenges still hinder the commercialization of DMFCs, such as inadequate cell performance and high catalyst loading, resulting in high cost. In this regard, developing more active catalysts for the methanol oxidation reaction (MOR) and developing cost-effective catalysts through efficient synthesis techniques is critical. Platinum (Pt) catalyst is commonly used because it can effectively catalyze the oxidation of methanol to CO_2 in an acidic environment as well as display reasonable stability under oxidative conditions.[3–5] However, the active sites of Pt are easily poisoned by strongly adsorbing methanol oxidation intermediates especially CO, thereby effectively lowering the fuel cell performance.[6,7]

A common strategy employed to overcome the above problem of catalyst poisoning is alloying Pt with elements that can promote the catalytic activity towards MOR.[8] The enhanced catalytic activity of such-modified surfaces over pure platinum can be ascribed to (i) bifunctional mechanism in which the second metal such as Ru provides oxygen-containing species by which water dissociates at relatively low potential for CO removal, and thereby combines with Pt in a synergic way to yield a more catalytically active surface; (ii) the ligand or the electronic effect, in which the second metal alters the electronic properties of Pt that cause the reduction in Pt-CO bond strength, thereby facilitating easy CO oxidation and thus yielding more active catalytic surface and (iii) the geometric effect, in which the second metal is assumed to be inactive and only plays the role of support which can improve the active surface area as well as expose suitable facets of Pt.[4,9,10] Furthermore, the introduction of relatively cheaper secondary metals can help to reduce the usage of expensive Pt catalyst and thereby lower the cost while maintaining good performance towards methanol oxidation.

There are numerous reports on Pt-based bimetallic electrocatalysts used in fuel cells which involves alloying Pt with elements such as ruthenium (Ru),[11,12] tin (Sn),[13,14] palladium (Pd),[15,16] nickel (Ni),[17,18] silver (Ag),[19,20] etc. Among the secondary metals, Pd, Ru, and Sn are widely employed for MOR. Pd is considered suitable mainly because of the very similar size and lattice structure with only less than 1% lattice mismatch.[21] On the other hand, Ru and Sn are preferred because of the enhanced active OH_{ads} species available on Ru and Sn sites at lower potentials, which will help oxidize the adsorbed CO to CO_2.[22,23]

Studies comparing the performance of these bimetallic catalysts prepared on carbon-based supports by different synthesis techniques have been extensively reported for the oxidation of various small organic molecules.[24–26] Most of these reports have widely employed synthesis techniques such as polyol, microemulsion, impregnation, colloidal methods, etc to prepare catalysts on carbon-based support mainly due to their advantageous control of morphology, size, and composition.[27] Moreover, surfactant/capping agents are also necessary during synthesis to achieve uniformity in the size or morphology of the catalysts, and the removal of these surfactant/capping agents is tedious as well as time-consuming and often has a destructive effect by blocking the catalyst's active sites.[28] Furthermore, electrode fabrication using these catalysts requires additional catalyst layer preparation methods like spraying, brush coating, drum-roll coating, and screen printing, which can cause wastage of the catalyst and reduction in catalyst performance.[29]

In this view, electrochemical deposition is a more beneficial catalyst preparation technique for actual practical applications as it can deposit directly on conductive support at locations having both ionic and electronic accessibility[30,31] making it a single-step procedure for preparing catalysts and fabricating electrodes as opposed to the case of multiple steps for chemical synthesis techniques. Electrodeposition offers the ability to easily tune the features of the catalysts by simply modifying the electrodeposition technique and parameters[32] while ensuring a thin layer of catalyst is prepared which is beneficial in lowering the internal resistance as well as improving the effective utilization of catalysts.[33]

As an alternative to corrosion-prone carbon support, Ti-based materials have been considered as potential alternative support due to their corrosion resistance, low cost and strong metal-support interaction (SMSI).[34] The investigation of bimetallic catalysts fabricated through the electrodeposition process onto Ti-based substrate towards MOR in DMFC is limited in the literature. Taking this into consideration, the present study is intended to prepare Pt-based bimetallic catalysts such as PtPd, PtSn, and PtRu electrodeposited on a titanium substrate and investigate the effect of secondary metal and its composition towards MOR and identify

*Electrochemical Society Member.
[z]E-mail: raghuc@iitm.ac.in

possible Pt-based catalysts of high catalytic activity and durability towards MOR with reduced CO poisoning.

Experimental

Titanium substrate pretreatment.—Titanium substrates were cut in an L-shape with a working area of 1 cm × 1 cm. The remaining area of the electrode acted as provision for electrical connections and was shielded with Teflon tape, thereby making a geometrical area of 2 cm^2 (both sides) available to the electrolyte solution. Ti foil was first cleaned with Millipore water and then mechanically polished with emery papers of medium roughness. The polished electrodes were sequentially cleaned using acetone, isopropanol, and Millipore water by sonicating in each solvent for five minutes. Further, the foil was pretreated by dipping for one minute in 5 wt% oxalic acid solution at 100 °C, which helped in cleaning the foil and obtaining a smooth oxide-free substrate surface.[35]

Electrodeposition of Pt and Pt-based electrodes.—The deposition of the catalyst was carried out on the pretreated Ti support using the corresponding metal precursor. H_2PtCl_6, $PdCl_2$, $RuCl_3$, and $SnCl_2$ were employed as precursors for Pt, Pd, Ru, and Sn. Pt and Ag/AgCl were used as the counter and reference electrodes, respectively. Galvanostatic pulse electrodeposition was used to deposit noble metal on Ti using rectangular current pulses. During each pulse, a reduction current was applied for 10 ms (t_{on}), followed by a relaxation time (t_{off}) of 90 ms where no current was applied, which corresponds to a duty cycle of 10%. The pulse amplitude applied during t_{on} period was different for each metal system and was chosen so as to apply a suitable deposition overpotential for the same metal loading. A schematic of the current pulse shape utilized for the electrodeposition process is shown in Fig. S1 (available online at stacks.iop.org/JES/167/024512/mmedia).

For the purpose of comparison, electrodeposition was performed such that a theoretical total metal loading of 0.65 mg cm^{-2} was achieved assuming 100% faradaic efficiency for deposition. Pulse deposition experiments were performed at room temperature on an SP-150 series electrochemical workstation (Biologic Science Instruments). By this technique, the high current density during the t_{on} period increased the number of nucleation sites on the substrate. The relaxation time (zero current density, t_{off}) improved the homogeneity of the deposition and limited hydrogen evolution.[36] In a bid to determine the optimum composition, bimetallic catalysts were prepared such that the composition ratio for Pt to secondary metal (Pd, Ru, and Sn) was 1:1, 2:1, and 3:1. Apart from the bimetallic catalyst, monometallic catalysts viz. Pt, Pd, Ru, and Sn were also electrodeposited on pretreated bare Ti substrate for comparison. All potentials quoted in this work are referred to a standard hydrogen electrode (SHE).

Physical and electrochemical characterization.—The synthesized electrodes were physically characterized by X-ray diffraction (XRD) (Bruker D8 Discover X-ray diffractometer, Cu-Kα source, $\lambda = 1.5406$ A°) and field emission high-resolution SEM (Hitachi S4800). Energy dispersive X-ray (EDX) analysis was performed to confirm the presence and composition as well as the distribution of metals on the Ti support. Electrochemical characterization experiments (viz. cyclic voltammetry and chronoamperometry) were performed at room temperature on the SP-150 series electrochemical workstation. All experiments were run in triplicate to ensure the reproducibility of the data. The electrochemically active surface area (ECSA) of Pt-based catalysts was determined by cyclic voltammetry in nitrogen-saturated 0.5 M H_2SO_4 by scanning between 0 to 1.4 V at a sweep rate of 50 mV s^{-1} and at room temperature. The area used for the calculation of ECSA was taken as 2 cm^2 since both sides (each of 1 cm^2) were exposed to the electrolyte during electrodeposition. The bimetallic catalysts were prepared in such a way that Pt was replaced with a second metal like Ru, Sn or Pd by keeping the total metal loading constant, similar to the Pt/Ti catalyst. To observe a fair comparison of performance between the prepared catalysts, the ECSA was normalized to the total metal loading of 0.65 mg cm^{-2}.

CO stripping voltammograms were conducted in 0.5 M H_2SO_4 solution, in which carbon monoxide (CO) was pre-adsorbed on the electrodes. Initially, CO was bubbled into 0.5 M H_2SO_4 for 20 min while the electrode potential was fixed at 0.1 V. Then, the dissolved CO in the solution was removed by bubbling N_2 into the solution and the stripping voltammograms were collected at a scan rate of 50 mV s^{-1}. The activity towards methanol oxidation was studied in nitrogen-saturated 0.5 M H_2SO_4 with 1 M CH_3OH solution by scanning the potential from 0 to 1.4 V. The catalytic activity was normalized to the geometric area of 2 cm^2. Electrochemical impedance spectroscopy (EIS) was carried out to understand the charge transfer properties of the electrodes. The Nyquist plots were obtained by applying a sinusoidal potential of 10 mV at frequencies from 100 kHz to 100 mHz while applying a potential of 0.6 V for the electrodeposited electrodes. Short-term stability of the electrocatalysts was investigated by performing chronoamperometry at 0.9 V for 30 min in nitrogen-saturated 0.5 M H_2SO_4 with 1 M CH_3OH solution. In order to investigate the electrocatalyst durability, accelerated durability tests (ADT) were conducted on prepared electrocatalysts by performing continuous potential cycling between 0.6 and 1.2 V for 1000 cycles at a scan rate of 50 mV s^{-1} with periodic measurements of ECSA and MOR activity after every 100 cycles.

Results and Discussion

Physical characterization.—Galvanostatic pulse electrodeposition was employed as the synthesis technique to prepare electrodeposited catalysts because the pulse deposition can ensure higher deposition rates along with minimized depletion layer thickness.[37] Pulse electrodeposition employed in this work for the preparation of all catalysts was performed at a 10% duty cycle and 10 Hz pulse frequency unless otherwise specified. The duration of deposition was determined by the deposition charge for the metal to achieve the expected composition and loading of the catalysts. The deposition parameters for each of the prepared catalysts are tabulated in Table SI.

Initially, Pt was deposited on the Ti substrate by employing a pulse current amplitude of 2.5 mA cm^{-2} using a solution of 2 mM H_2PtCl_6 and 10 mM H_2SO_4. Scanning electron microscope images presented in Fig. S2 show the morphology of Pt electrodes prepared, which shows that the Pt deposit has a smooth globular structure uniformly distributed on the Ti substrate.

For the preparation of bimetallic catalysts, the deposition was sequentially performed in order to mimic the formation of a core–shell structure by depositing a secondary metal as the inner core while Pt was prepared as the outer shell. Such core–shell catalysts offer interesting properties because of the possible synergistic interaction between the core and shell. The shell provides sites for catalytic activity while the core element possibly exerts an electronic effect on the shell element and can induce greater suppression of adsorbed poisonous species.[38]

PtPd catalysts were prepared by initially depositing Pd from a solution of 2 mM $PdCl_2$ and 0.1 M $HClO_4$ using pulse current amplitude of 1.6 mA cm^{-2}, followed by Pt deposition using pulse current amplitude of 2.5 mA cm^{-2} using a solution of 2 mM H_2PtCl_6 and 10 mM H_2SO_4. The various compositions of PtPd prepared are denoted as $Pt_{50}Pd_{50}$/Ti, $Pt_{67}Pd_{33}$/Ti, and $Pt_{75}Pd_{25}$/Ti where the subscripts indicate the percentage of the component in the composite catalyst. Pure Pd/Ti was also prepared for comparison.

SEM images of the sequentially deposited PtPd/Ti were compared with electrodeposited Pd/Ti in Fig. 1. The Pd particles in Pd/Ti showed sharp dendritic morphology with several thin branches from long stems as can be observed in Fig. 1a. On the other hand, the deposition of Pt over the Pd structures resulted in a change of morphology to nanoflower structure because of the increased number of shorter branches connecting to the main stem as can be

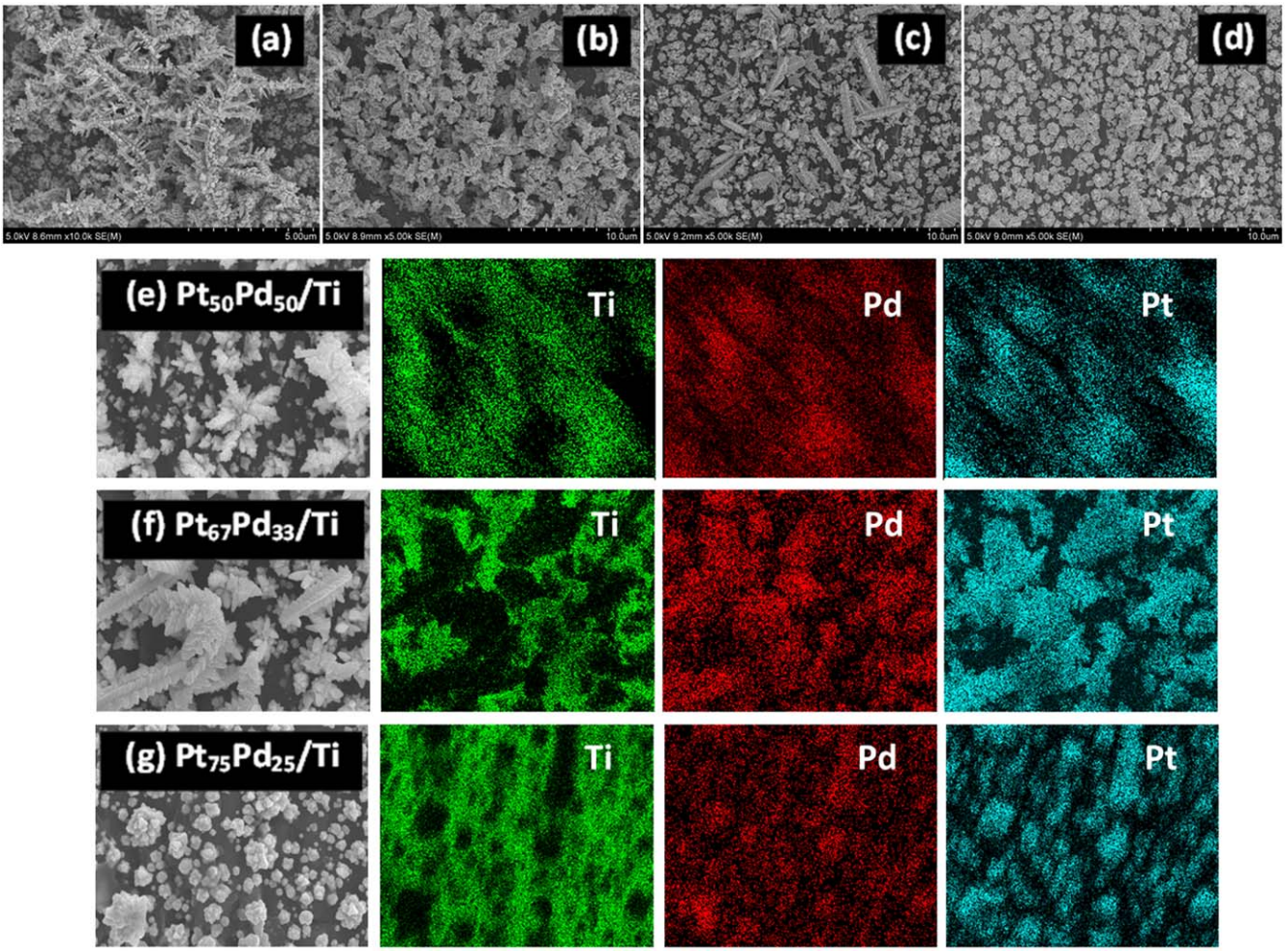

Figure 1. Scanning electron microscope images of (a) Pd/Ti and PtPd electrodeposited on Ti substrate of different composition ratios viz. (b) $Pt_{50}Pd_{50}$/Ti, (c) $Pt_{67}Pd_{33}$/Ti and (d) $Pt_{75}Pd_{25}$/Ti; Elemental mapping of PtPd electrodeposited on Ti substrate of different composition ratios viz.: (e) $Pt_{50}Pd_{50}$/Ti, (f) $Pt_{67}Pd_{33}$/Ti and (g) $Pt_{75}Pd_{25}$/Ti.

seen in Figs. 1b–1d. Higher magnification images of the PtPd catalysts are shown in Fig. S3. Close observation of the images implies that Pt deposition resulted in thickening of the dendritic branches as the ratio of Pt to Pd is changed from 1:1, 2:1 to 3:1 thereby suggesting that the thickening could be ascribed to the increased deposition of Pt on the Pd dendrites.

The EDX spectrum of catalysts is shown in Fig. S4 while the EDX mapping of the catalysts is shown in Figs. 1e–1g. The relative surface content of the metals for the PtPd electrocatalysts determined from the EDX spectrum is tabulated in Table SII. EDX mapping clearly illustrates the deposit comprised of Pt and Pd, and the distribution of both the metals remains uniform along with the structure for all compositions of PtPd. The elemental distribution was found to be consistent with the expected composition for PtPd electrocatalysts.

Similar to PtPd preparation, the PtSn bimetallic electrodes were prepared by sequentially depositing Sn as the inner core, while Pt was prepared as the outer shell. Sn ions tend to form oxides in aqueous acidic solutions. Therefore, a complexing agent, citrate salt, was added to ensure the solubility of the Sn^{2+} ions. Sn was deposited from an electrolyte containing 10 mM $SnCl_2$ precursor and 50 mM sodium citrate with 10 mM H_2SO_4 as supporting electrolyte while Pt was deposited using an electrolyte containing 2 mM H_2PtCl_6 + 10 mM H_2SO_4.

At first, Sn was deposited on a Ti substrate using pulse current amplitude of 40 mA cm^{-2}. Pt was deposited over the Sn deposits with pulse current amplitude of 2.5 mA cm^{-2}. The various compositions of PtSn which were prepared include $Pt_{50}Sn_{50}$/Ti, $Pt_{67}Sn_{33}$/Ti, and $Pt_{75}Sn_{25}$/Ti, where the subscripts indicate the percentage of the component in the composite catalyst. Pure Sn/Ti was also prepared for comparison.

SEM images of the sequentially deposited PtSn/Ti were compared with the electrodeposited Sn/Ti in Fig. 2. The Sn deposited in Sn/Ti was porous with a relatively uniform arrangement of particles with sharp features as shown in Fig. 2a. On the deposition of Pt on Sn deposits, the particles became irregularly shaped and the particle size relatively increased with an increase in Pt to Sn ratio as can be seen in Figs. 2b–2d. Higher magnification images of the PtSn catalysts are shown in Fig. S5. EDX analysis and mapping were carried out to determine the distribution of the PtSn catalysts on the Ti substrate and are shown in Fig. S6 and Figs. 2e–2f, respectively while the surface composition is tabulated in Table SIII. The elemental distribution was found to be in agreement with the expected target composition for PtSn electrocatalysts.

In the case of preparation of PtRu catalysts, sequential deposition of Ru and Pt did not show promising performance for methanol oxidation during trial experiments, and the activity resembled that of Pt. Nevertheless, surface composition consistent with overall composition was reported to be more effective for active PtRu catalysts towards methanol oxidation.[39] Hence, to achieve uniform surface composition, a co-deposition route was adopted to prepare the PtRu bimetallic electrocatalyst onto the Ti substrate. Pulse current waveform with a pulse amplitude of 2.5 mA cm^{-2} was employed for the co-deposition of PtRu from a solution containing the precursors of both the metal

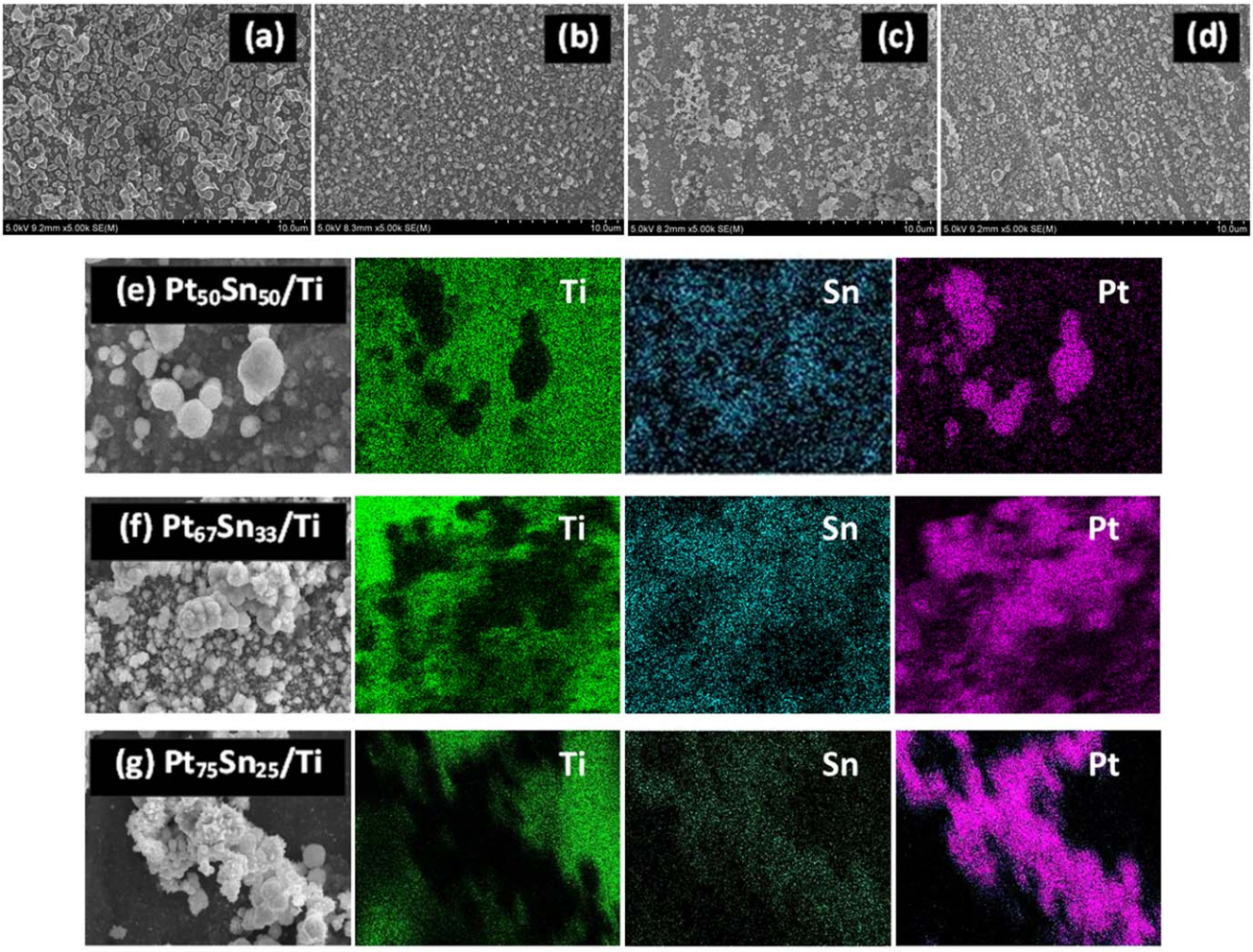

Figure 2. Scanning electron microscope images of (a) Sn/Ti and PtSn electrodeposited on Ti substrate of different composition ratios viz. (b) $Pt_{50}Sn_{50}$/Ti, (c) $Pt_{67}Sn_{33}$/Ti and (d) $Pt_{75}Sn_{25}$/Ti; Elemental mapping of PtSn electrodeposited on Ti substrate of different composition ratios viz. (e) $Pt_{50}Sn_{50}$/Ti, (f) $Pt_{67}Sn_{33}$/Ti and (g) $Pt_{75}Sn_{25}$/Ti.

atoms. The concentration of Pt and Ru metal precursors were taken in such a way to achieve the desired composition of PtRu bimetallic electrocatalyst. Besides this, the duration of deposition was determined by the deposition charge for the metal to achieve the expected composition of PtRu. The deposition parameters are tabulated in Table SI. The various compositions of PtRu which were prepared include $Pt_{50}Ru_{50}$/Ti, $Pt_{67}Ru_{33}$/Ti, and $Pt_{75}Ru_{25}$/Ti, where the subscripts indicate the percentage of the component in the composite catalyst. For the purpose of comparison, pure Ru on Ti substrate (with Ru loading of 0.65 mg cm^{-2}) was also prepared from an electrolyte solution containing 4 mM $RuCl_3$ in 10 mM H_2SO_4. The pulse waveform applied for Ru deposition on Ti was similar to that used for the co-deposition of PtRu.

SEM images of the co-deposited PtRu/Ti are compared with electrodeposited Ru/Ti in Fig. 3, with higher magnification images of the PtRu catalysts shown in Fig. S7. Ru particles in Ru/Ti were observed to have an agglomerated spherical morphology which was uniformly distributed on the Ti substrate as can be seen in Fig. 3a. However, when Pt and Ru are co-deposited, larger particles are formed which cover the substrate uniformly as can be seen in Figs. 3b–3d. The PtRu electrodes having Pt to Ru ratio of 1:1 and 2:1 have a spherical morphology while the ratio of 3:1 has catalyst clusters growing on top of each other. Hence, a change could be observed in the overall catalyst layer from smooth to a porous layer which could be attributed to the stronger self-agglomeration of Pt particles at higher Pt to Ru composition ratio.[40]

EDX analysis was carried out to determine the distribution of the PtRu catalysts on the Ti substrate. The EDX spectrum of PtRu catalysts is shown in Fig. S8 while the EDX mapping of the catalysts is shown in Figs. 3e–3g. The relative surface content of the metals for the PtRu electrocatalysts determined from the EDX spectrum is tabulated in Table SIV. EDX mappings clearly indicate a uniform distribution of Pt and Ru throughout the substrate. The distribution of elements appeared close to the expected composition for PtRu electrocatalysts.

XRD patterns of the electrodeposited bimetallic electrocatalysts are displayed in Fig. 4. The XRD pattern for Pt/Ti is also included for comparison. It can be seen that all electrocatalysts show characteristic peaks at 2θ ~46°, 68°, and 82° which correspond to the lattice planes (200), (220), and (311) of the face-centered cubic (fcc) structured platinum (JCPDS No. 04–0802). The peak at 2θ ~40° corresponding to the Pt (111) plane overlaps with that of the Ti substrate peak (2θ = 40.170), as reported in the literature.[41] Broadening of XRD peaks and a slight shift of Bragg angle may suggest the formation of bimetallic alloy, however, it cannot be considered as conclusive evidence because there may be confusion as to whether the peaks are arising from the mixture of fcc Pt and binary catalyst, or a mix between fcc Pt and bimetallic alloy.[42] Crystallite sizes were calculated based on Pt (200) peak using the Scherrer equation and are tabulated in Table SV. Among the PtPd bimetallic catalysts shown in Fig. 4a, the crystallite size is smallest for $Pt_{50}Pd_{50}$/Ti (7.8 nm) compared to $Pt_{67}Pd_{33}$/Ti (11.4 nm) and

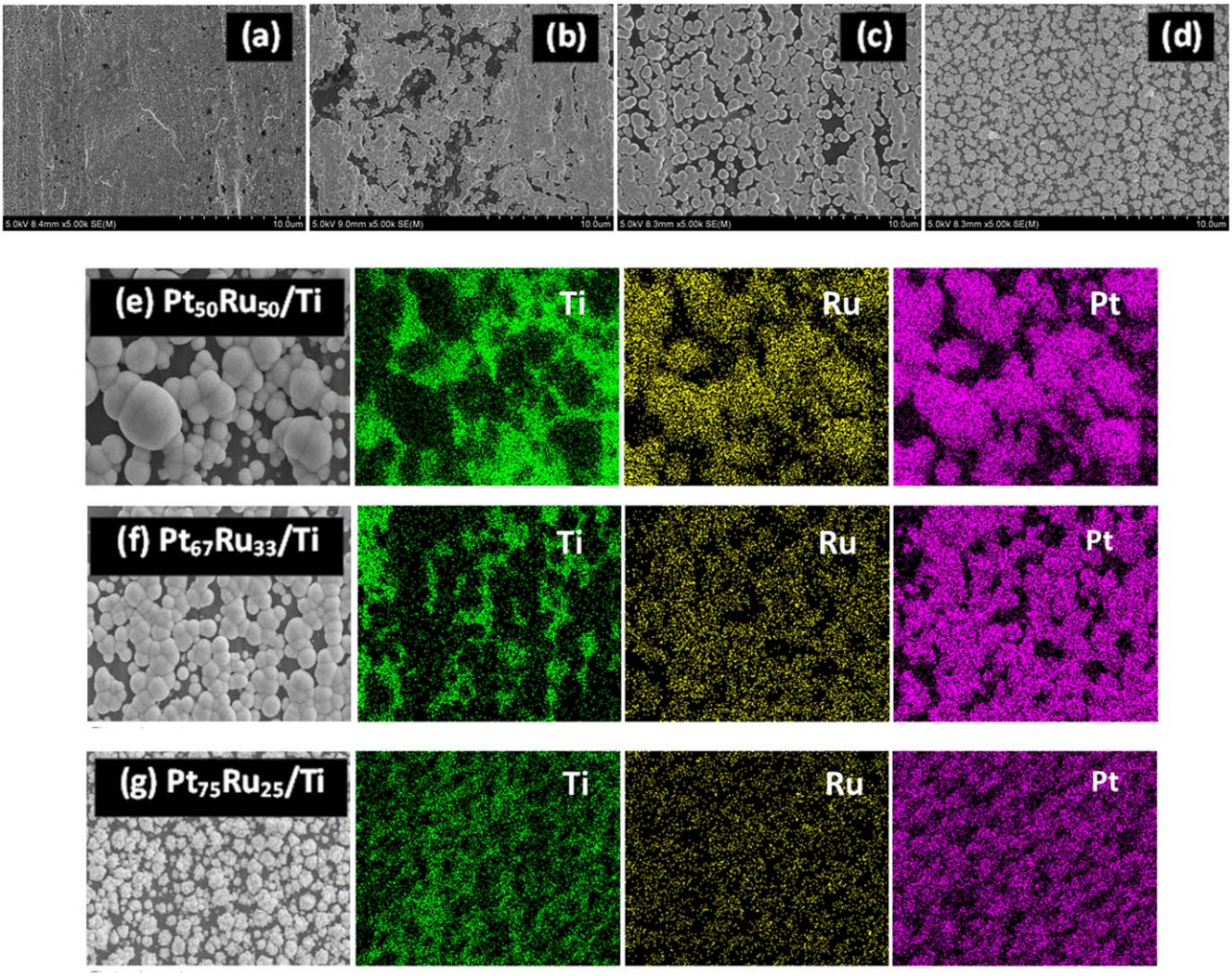

Figure 3. Scanning electron microscope images of (a) Ru/Ti and PtRu electrodeposited on Ti substrate of different composition ratios viz. (b) $Pt_{50}Ru_{50}$/Ti, (c) $Pt_{67}Ru_{33}$/Ti and (d) $Pt_{75}Ru_{25}$/Ti; Elemental mapping of PtRu electrodeposited on Ti substrate of different composition ratios viz. (e) $Pt_{50}Ru_{50}$/Ti, (f) $Pt_{67}Ru_{33}$/Ti and (g) $Pt_{75}Ru_{25}$/Ti.

$Pt_{75}Pd_{25}$/Ti (10.1 nm). In case of the PtSn bimetallic catalysts as shown in Fig. 4b, the crystallite size was smallest for $Pt_{75}Sn_{25}$/Ti (12.3 nm) compared to $Pt_{50}Sn_{50}$/Ti (27.3 nm) and $Pt_{67}Sn_{33}$/Ti (14.7 nm), while for the PtRu bimetallic catalysts shown in Fig. 4c, the crystallite sizes were more or less close to 6 nm.

Electrochemical characterization.—Electrochemical surface area (ECSA) of the deposited catalysts was determined by evaluating the hydrogen adsorption/desorption (ads/des) charge obtained from cyclic voltammetry performed in 0.5 M H_2SO_4 in the potential range of 0 to 1.4 V at a scan rate of 50 mV s^{-1}. Figure S9a shows the cyclic voltammogram observed for the electrodeposited Pt catalyst. The cyclic voltammogram in 0.5 M H_2SO_4 for the Pt exhibit the characteristic features of polycrystalline Pt in sulphuric acid electrolyte.[43] Two well-defined hydrogen adsorption peaks at about 0.1 V and 0.2 V were observed, which are respectively attributed to the surface adsorption characteristics of Pt(110) and Pt(100) facets.[44] The ECSA of the electrode was calculated using hydrogen ads/des peaks from the cyclic voltammograms using the formula:

$$ECSA = \frac{Q_H}{m^* Q_C}$$

where Q_H is integrated hydrogen ads/des charge, m is the metal loading and Q_C is the hydrogen ads/des charge on a smooth platinum electrode (210 μC cm^{-2}). The activity of electrodeposited Pt/Ti catalysts towards methanol oxidation was determined from the cyclic voltammetry in a nitrogen-saturated 1 M CH_3OH in 0.5 M H_2SO_4 solution at a scan rate of 50 mV s^{-1} and is shown in Fig. S9b. As expected, the forward scan of Pt/Ti electrodes are characterized by a strong current peak at ~1.0 V and another peak in the backward scan at around ~0.8 V, characteristic for the oxidation of intermediate adsorbed on the electrode surface in the forward scan.

The ECSA of PtPd/Ti electrodes, as well as the Pd/Ti electrode, were also examined and results are shown in Fig. 5a. It can be observed that the Pd/Ti prepared for comparison also exhibit well-known hydrogen ads/des peaks in the potential region of 0 to 0.2 V and Pd oxide formation and reduction within the region of 0.6 to 1.4 V, which is indicative of the predominant Pd metal surface electrochemistry,[45] while the PtPd/Ti electrodes exhibit characteristic Pt and Pd electrochemical behavior. The analysis shows that PtPd/Ti electrodes exhibited relatively similar ECSA values, with $Pt_{67}Pd_{33}$/Ti offering the highest ECSA of ~27 m^2 g^{-1} among the prepared electrodes while Pd/Ti showed an ECSA of ~16 m^2 g^{-1}. The ECSA values of all the catalysts are tabulated in Table SVI.

To further confirm the ECSA of the PtPd/Ti electrodes, CO stripping voltammetry was performed and the observed voltammograms are shown in Fig. 5b. The ECSA values obtained from the CO stripping voltammogram are tabulated in Table SVI and are found to

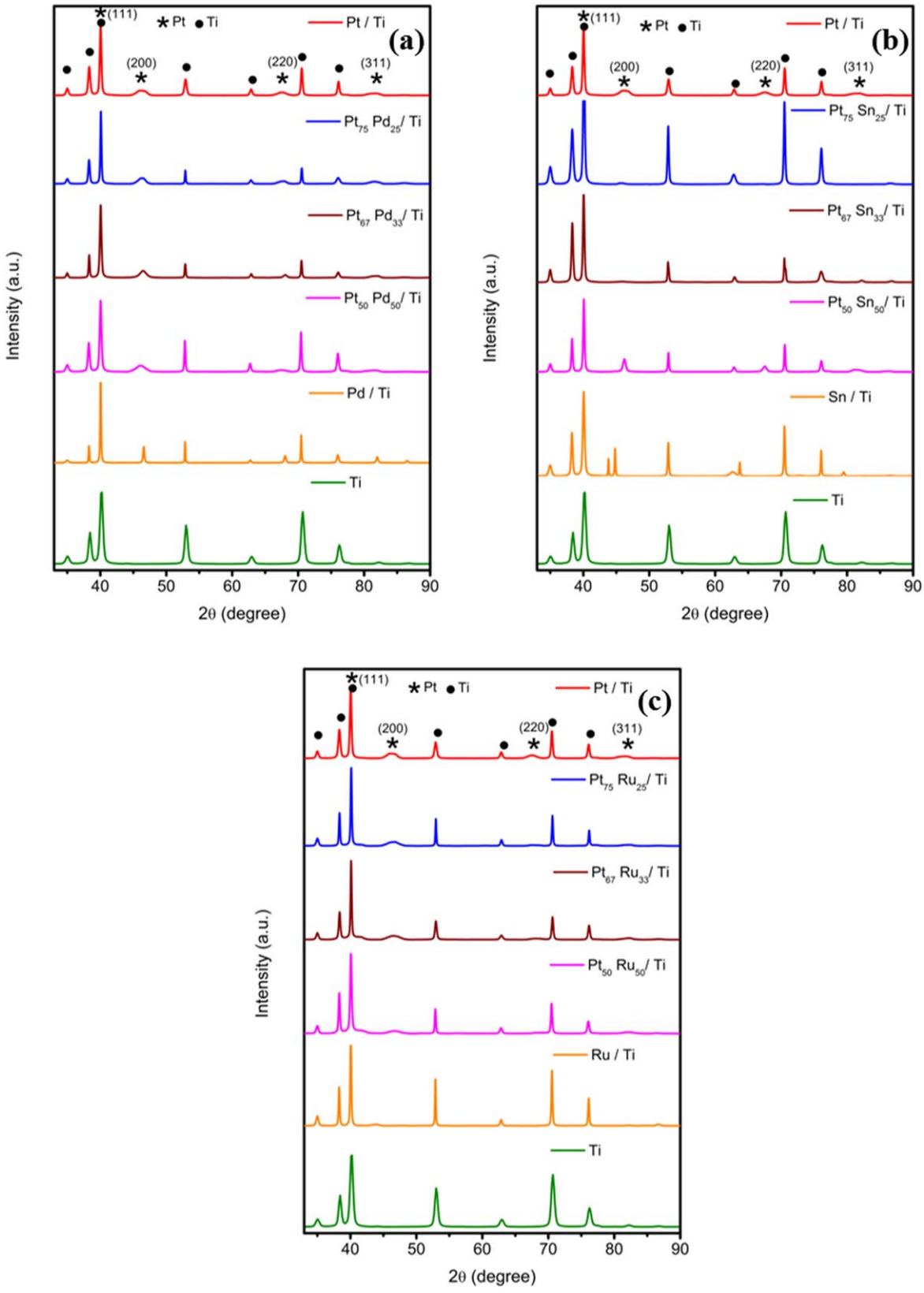

Figure 4. XRD pattern comparing Pt with (a) PtPd, (b) PtSn and (c) PtRu bimetallic catalysts prepared by electrodeposition on Ti substrate.

be in relatively good agreement with those obtained from hydrogen ads/des experiments. All stripping voltammograms show a CO oxidation peak which moves toward less positive potentials as Pd was replaced by Pt in the PtPd/Ti electrodes. This indicates the slightly easier oxidation of adsorbed CO on PtPd/Ti electrodes when compared to Pd/Ti. Furthermore, it can be observed that the PtPd/Ti electrodes exhibited a single CO oxidation peak which could be attributed to the synergistic effect of Pt and Pd.[46] In addition, the CO

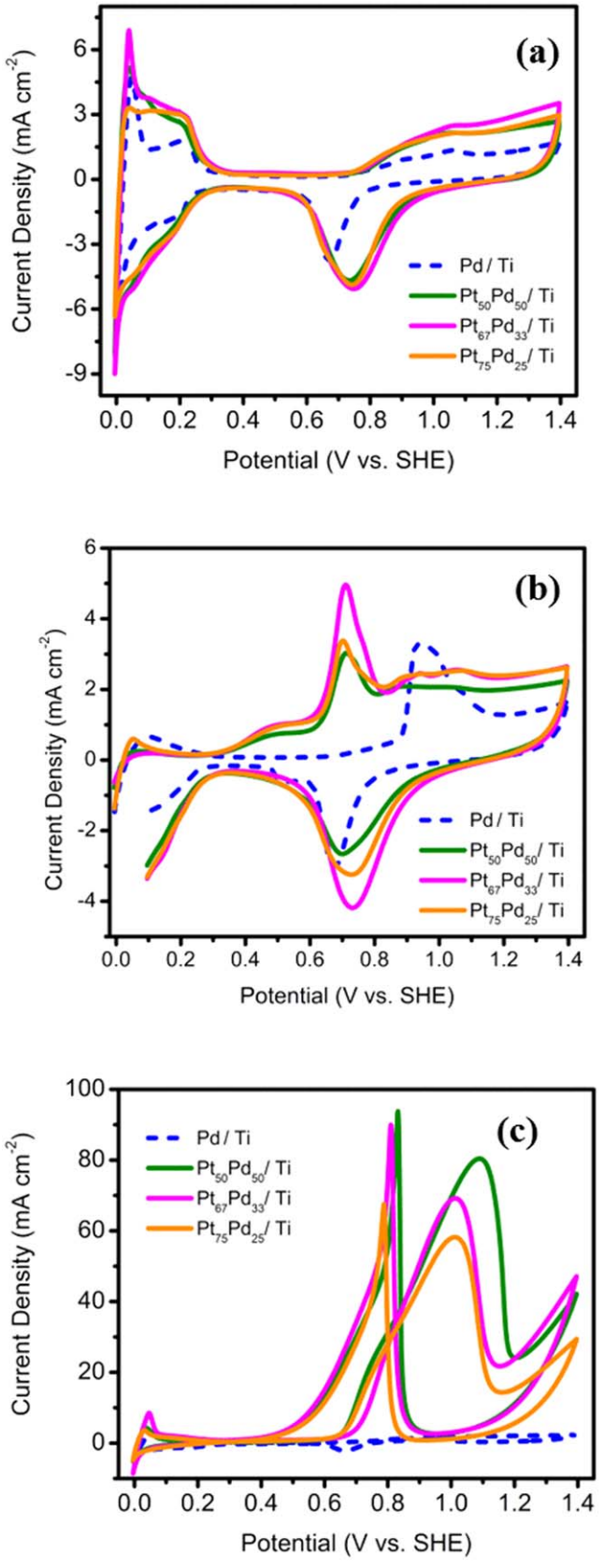

Figure 5. (a) Cyclic voltammogram of PtPd/Ti (solid lines) and Pd/Ti (dash line) electrodes in 0.5 M H_2SO_4 at a scan rate of 50 mV s^{-1}; (b) CO-stripping voltammograms of PtPd/Ti (solid lines) and Pd/Ti (dash line) electrodes in 0.5 M H_2SO_4 at a scan rate of 50 mV s^{-1}; (c) Cyclic voltammogram of PtPd/Ti (solid lines) and Pd/Ti (dash line) electrodes in 0.5 M H_2SO_4 + 1 M CH_3OH at a scan rate of 50 mV s^{-1}.

oxidation onset potentials of PtPd/Ti electrodes are significantly lower than the Pd/Ti electrode, suggesting an electronic modification affecting the CO adsorption characteristics on PtPd bimetallic catalyst when compared to pure Pd.[47] The activity of PtPd/Ti electrodes towards methanol oxidation was investigated by performing cyclic voltammetry in nitrogen saturated 1 M CH_3OH + 0.5 M H_2SO_4 at a sweep rate of 50 mV s^{-1} and at room temperature. It can be observed from Fig. 5c, that among the various compositions of PtPd/Ti, $Pt_{50}Pd_{50}$/Ti exhibited the highest activity towards methanol oxidation while Pd/Ti electrode offered almost negligible methanol oxidation activity.

EIS was carried out to understand the charge transfer properties of the electrodes. The Nyquist plots were obtained by applying a sinusoidal potential of 10 mV at frequencies from 100 kHz to 100 mHz while applying a potential of 0.6 V for the electrodeposited electrodes and can be represented with a Randle equivalent circuit, as shown in Fig. S10 where R_{soln} is the solution resistance, C_{dl} is the double layer capacitor and R_{ct} is the charge transfer resistance. Figure S11 shows the Nyquist plots obtained for the electrodeposited PtPd electrodes. The Nyquist plots are semi-circular shaped and the diameters of the impedance arcs of $Pt_{50}Pd_{50}$/Ti are much smaller than other PtPd/Ti electrodes which suggest faster electron-transfer kinetics with an increase in Pd content in the PtPd bimetallic electrodes.

Additionally, chronoamperometric measurements were conducted for evaluation of the catalytic stability of PtPd electrodes by applying 0.9 V in 1 M CH_3OH + 0.5 M H_2SO_4 solution for 30 min as shown in Fig. S12. All electrodes exhibited current decay during the initial period because of the formation of intermediate species on the electrocatalysts. However, the $Pt_{50}Pd_{50}$/Ti catalyst appears to have the lowest current decay after 30 min implying the electrode exhibits a stable activity for oxidizing methanol and tolerance against the poisoning by intermediates of methanol oxidation.

The comparison of the various parameters determined from the electrochemical analysis of electrodes are shown in Table SVI. Electrochemical characterization of the electrodes shows that PtPd/Ti electrode prepared with a catalyst ratio of 1:1 (i.e. $Pt_{50}Pd_{50}$/Ti) is found to exhibit higher performance among all electrodes towards methanol oxidation, which could be due to the catalytic function depending on the Pt shell thickness resulting in different extent of synergism between Pt and Pd. The results are consistent with findings in literature where PtPd bimetallic catalysts having Pt:Pd ratio of 1:1 showed excellent anti-CO poisoning property and high electrocatalytic performance towards MOR.[48,49] This implies that the Pd in the sequential deposition of Pt over Pd plays an important role in enhancing the performance towards methanol oxidation.

In the case of PtSn catalysts, cyclic voltammograms at 50 mV s^{-1} for Sn and PtSn surfaces in 0.5 M H_2SO_4 are shown in Fig. 6a. Sn and PtSn catalysts have a less-defined profile in the cyclic voltammogram. Furthermore, a substantial double-layer charge profile was observed for Sn and PtSn electrodes. Such behavior could be attributed to the oxophilic nature of Sn in the monometallic and bimetallic electrodes.[50] The ECSA of PtSn electrodes were examined by the hydrogen underpotential deposition method and is shown in Fig. 6a, where among the electrodes, $Pt_{75}Sn_{25}$/Ti exhibited the highest ECSA of ~14 m^2 g^{-1}. The ECSA for electrodes with Sn composition could better be determined by CO stripping voltammetry as shown in Fig. 6b. The $Pt_{75}Sn_{25}$/Ti electrode was observed to exhibit higher ECSA (~39 m^2 g^{-1}) compared to other composition electrodes.

Though pure Sn is readily oxidized and is not active for CO oxidation, the addition of Sn to Pt provides active sites for O_2 adsorption which thereby eases the CO oxidation as indicated by the relatively low onset potential of ~0.35 V during CO stripping voltammograms. In addition, a broader CO oxidation region between ~0.35 and 0.9 V was observed for the PtSn electrodes. The peak located at the lower potential can be associated to the PtSn interaction, whereas the one situated at higher potential can be

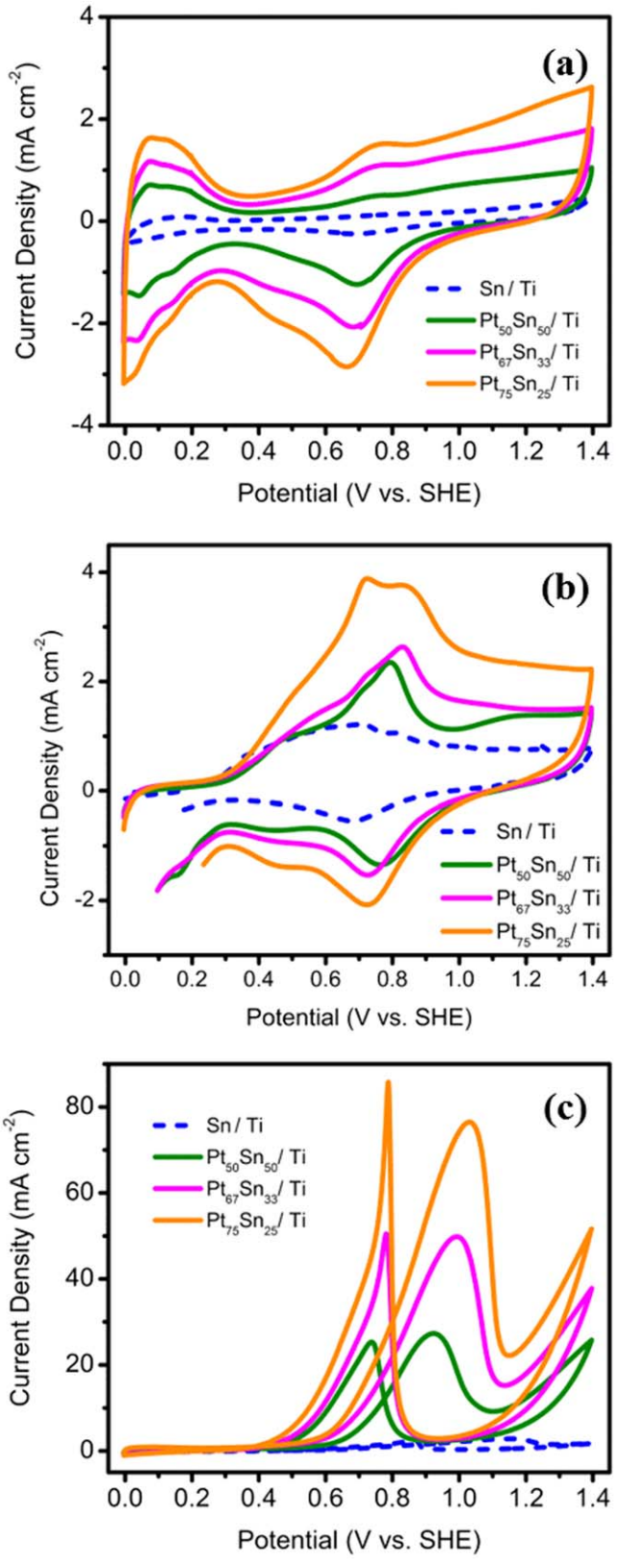

Figure 6. (a) Cyclic voltammogram of PtSn/Ti (solid lines) and Sn/Ti (dash line) electrodes in 0.5 M H_2SO_4 at a scan rate of 50 mV s^{-1}; (b) CO-stripping voltammograms of PtSn/Ti (solid lines) and Sn/Ti (dash line) electrodes in 0.5 M H_2SO_4 at a scan rate of 50 mV s^{-1}; (c) Cyclic voltammogram of PtSn/Ti (solid lines) and Sn/Ti (dash line) electrodes in 0.5 M H_2SO_4 + 1 M CH_3OH at a scan rate of 50 mV s^{-1}.

attributed to the Pt portion of the bimetallic electrode.[51] The combination of the bifunctional effect and the electronic ligand effect can contribute to the better CO tolerance of PtSn electrodes.

The activity of the electrodeposited PtSn catalysts towards methanol oxidation is shown in Fig. 6c. Though Sn/Ti exhibits some activity towards methanol oxidation, it is significantly lower than PtSn catalysts. It can be observed that the magnitude of the observed peak current density of methanol oxidation for the PtSn catalysts increased as the amount of Sn decreased, following the order of $Pt_{75}Sn_{25}$/Ti > $Pt_{66}Sn_{33}$/Ti > $Pt_{50}Sn_{50}$/Ti, with $Pt_{75}Sn_{25}$/Ti offering a peak current density of ~76 mA cm^{-2} during methanol oxidation.

The Nyquist plots of the PtSn/Ti electrodes shown in Fig. S13 indicate semicircles of smaller diameter observed with increasing Pt content in the PtSn bimetallic catalysts suggests faster electron-transfer kinetics at ratios with more Pt content. Additionally, analysis of catalysts stability by chronoamperometry as shown in Fig. S14 further corroborate the better stability of the $Pt_{75}Sn_{25}$/Ti compared to other compositions of PtSn electrodes.

The comparison of the various parameters determined from the electrochemical analysis of the various compositions of PtSn electrodes are shown in Table SVI. Electrochemical characterization of the electrodes shows that PtSn electrode prepared with a catalyst ratio of Pt to Sn atomic ratio of 3:1 (i.e. $Pt_{75}Sn_{25}$/Ti) was found to be the most optimum composition, exhibiting a significant CO tolerance as well as high electrocatalytic activity and stability toward methanol oxidation. This is in corroboration with the fact that PtSn in the ratio of 3:1 has been reported to be the optimum composition, which is most active and displays a strong synergistic effect in methanol electrooxidation.[52]

To investigate the performance of PtRu catalysts, cyclic voltammograms at 50 mV s^{-1} for Ru and different PtRu composition in 0.5 M H_2SO_4 were performed and are shown in Fig. 7a. Ru/Ti electrodes exhibit strong double-layer capacitance in the voltammogram indicative of the pseudocapacitive nature of Ru.[53] With decreasing Ru content in the binary catalysts the current-potential peaks in the hydrogen ads/des region, as well as a double layer, become narrow and more defined than on pure Ru. The ECSA of PtRu electrodes were examined by the hydrogen underpotential deposition method. It can be observed in Fig. 7a that the $Pt_{50}Ru_{50}$/Ti exhibited the highest ECSA of ~20 m^2 g^{-1} among the electrodes.

However, for electrodes with Ru composition, the determination of the ECSA by hydrogen underpotential deposition could be imprecise since Ru is found to have an overlap of the hydrogen and ruthenium oxidation currents.[54] Hence, to better determine the ECSA of the PtPd/Ti electrodes, CO stripping voltammetry was performed and the observed voltammograms are shown in Fig. 7b. The $Pt_{50}Ru_{50}$/Ti electrode was observed to exhibit higher ECSA of ~26 m^2 g^{-1} compared to other composition electrodes. Since the catalysts were prepared by replacing Pt with the second metal (Ru, Sn, Pd) in a manner that the total metal loading was kept constant at 0.65 mg cm^{-2} for the bimetallic catalysts, only a marginal increase in ECSA (m^2 g^{-1}) was observed between the Pt and bimetallic-Pt catalysts.

The voltammograms show a single CO oxidation peak with peak potential as well as onset potentials shifting to more negative potentials with more Ru in the PtRu bimetallic electrodes. This clearly indicates the easier oxidation of adsorbed CO because Ru in the PtRu electrodes supplies oxygen species for CO oxidation.[55] The activity of the PtRu electrodeposited catalysts towards methanol oxidation was studied using cyclic voltammetry in the potential range of 0 to 1.4 V at a scan rate of 50 mV s^{-1}. Ru/Ti offered almost negligible activity towards methanol oxidation. Analysis of the forward peak current densities from Fig. 7c indicate that the PtRu bimetallic electrodes offered methanol oxidation activity in the order of $Pt_{50}Ru_{50}$/Ti > $Pt_{67}Ru_{33}$/Ti > $Pt_{75}Ru_{26}$/Ti electrode.

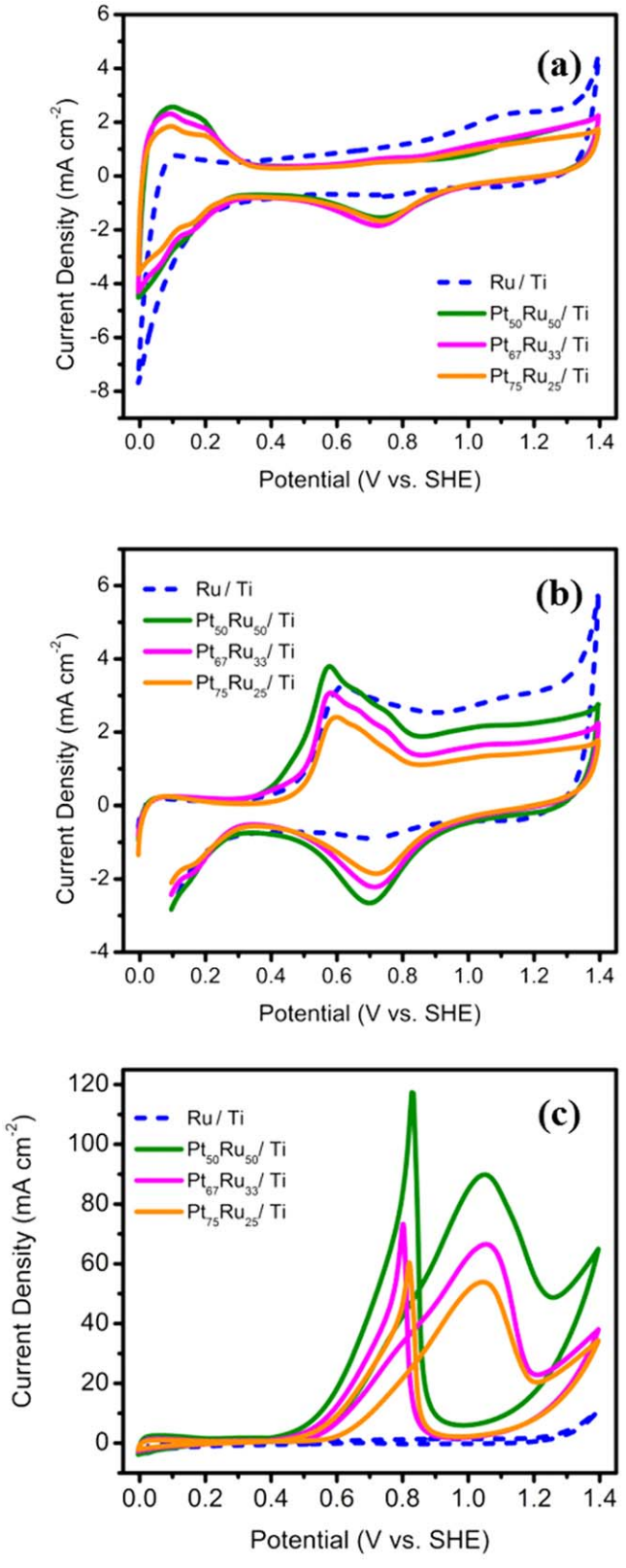

Figure 7. (a) Cyclic voltammogram of PtRu/Ti (solid lines) and Ru/Ti (dash line) electrodes in 0.5 M H_2SO_4 at a scan rate of 50 mV s^{-1}; (b) CO-stripping voltammograms of PtRu/Ti (solid lines) and Ru/Ti (dash line) electrodes in 0.5 M H_2SO_4 at a scan rate of 50 mV s^{-1}; (c) Cyclic voltammogram of PtRu/Ti (solid lines) and Ru/Ti (dash line) electrodes in 1 M CH_3OH + 0.5 M H_2SO_4 at a scan rate of 50 mV s^{-1}.

The Nyquist plots of the PtRu/Ti electrodes are shown in Fig. S15. The observed semicircles indicate the $Pt_{50}Ru_{50}$/Ti have a smaller diameter than other PtRu/Ti electrodes which suggests faster electron-transfer kinetics with an increase in Ru content in the PtRu bimetallic composite electrodes. Moreover, the stability of the PtRu/Ti is evaluated by chronoamperometry curves as shown in Fig. S16 and it is evident that $Pt_{50}Ru_{50}$/Ti exhibits better stability than other compositions of PtRu electrodes.

The comparison of the various parameters determined from the electrochemical analysis of the various compositions of PtRu electrodes are shown in Table SVI. Electrochemical characterization of the electrodes shows that PtRu electrode prepared with a catalyst ratio of 1:1 (i.e. $Pt_{50}Ru_{50}$/Ti) was found to show higher performance among all electrodes towards methanol oxidation which could be related to their superior CO tolerance through the bifunctional mechanism. This optimum composition of Pt to Ru atomic ratio of 1:1 is consistent with literature reports to be the most active and displays a strong synergistic effect in methanol electrooxidation.[52]

Comparison of electrochemical performance of bimetallic catalysts.—The various compositions of the binary electrodes of PtPd, PtRu, and PtSn exhibit good performance and show a significant change in activity on modifying the composition and components. This clearly reveals that the activity of Pt-based bimetallic catalysts towards methanol oxidation depends clearly on the choice of secondary metal and its composition. A comparison of Pt and Pt-based bimetallic (PtRu, PtPd, and PtSn) electrocatalyst performance towards methanol oxidation reported in the literature is presented in Table SVII.

For the purpose of better understanding, the highly active composition of PtPd, PtRu, and PtSn are compared with Pt. Figure 8a shows the comparison of cyclic voltammograms in 0.5 M H_2SO_4 at 50 mV s^{-1}. PtRu/Ti and PtSn/Ti show less well defined H_2 adsorption and desorption peaks and exhibit strong double-layer capacitance compared to PtPd/Ti and Pt/Ti which are indicative of the oxophilic nature of Ru and Sn.

The CO-stripping voltammetry measurements shown in Fig. 8b indicate that the addition of binary metal to platinum led to a decrease in the CO-stripping onset potential confirming that the electronic effect of Pd, Ru, and Sn can influence the Pt-CO bond strength and help to free active Pt surface. The onset potentials for CO-stripping follow the order of PtSn/Ti < PtRu/Ti < PtPd/Ti < Pt/Ti with the onset potential values of 0.362, 0.381, 0.601, and 0.605 V for $Pt_{75}Sn_{25}$/Ti, $Pt_{50}Ru_{50}$/Ti, $Pt_{50}Pd_{50}$/Ti, and Pt/Ti, respectively which clearly indicates that the binding energy of CO on Pt sites available on PtRu and PtSn bimetallic surfaces was lower than that on pure Pt as well as on PtPd. This could be ascribed to the bifunctional mechanism commonly observed in Ru and Sn where the oxophilic nature of Ru and Sn can provide necessary –OH groups to easily oxidize CO.

The comparison of cyclic voltammograms for methanol oxidation in 0.5 M H_2SO_4 + 1 M CH_3OH is shown in Fig. 8c. The Pt-based bimetallic catalysts perform better than Pt toward methanol oxidation. The magnitude of the observed peak current density of MOR follows the order PtRu/Ti > PtPd/Ti > PtSn/Ti > Pt/Ti with the peak current density values of 89.84, 80.42, 76.47, and 68.34 mA cm^{-2} for $Pt_{50}Ru_{50}$/Ti, $Pt_{50}Pd_{50}$/Ti, $Pt_{75}Sn_{25}$/Ti, and Pt/Ti, respectively. This suggests that PtRu is a better-performing bimetallic catalyst towards MOR compared to PtPd and PtSn. Additionally, the onset potential for MOR was compared to understand the kinetics of MOR in the binary catalysts. PtPd/Ti (0.665 V) did not show significant change in onset potential for MOR compared to Pt/Ti, while the onset for PtRu/Ti (0.545 V) and PtSn/Ti (0.601 V) are shifted significantly to lower values compared to Pt/Ti (0.659 V). This could signify that methanol oxidation commences at the lower potential on PtRu and PtSn compared to

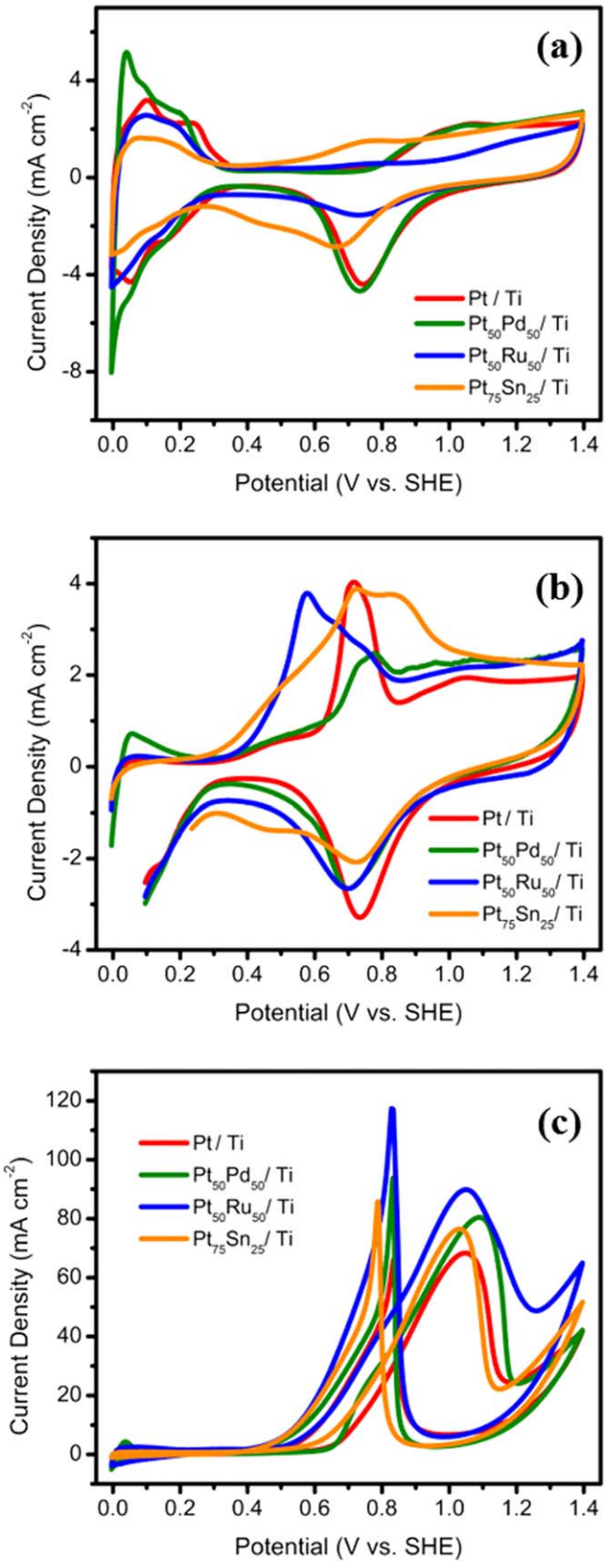

Figure 8. (a) Comparison of cyclic voltammogram of Pt/Ti with most active composition of PtPd/Ti, PtRu/Ti and PtSn/Ti electrodes in 0.5 M H_2SO_4 at a scan rate of 50 mV s^{-1}; (b) Comparison of CO-stripping voltammograms of Pt/Ti with most active composition of PtPd/Ti, PtRu/Ti and PtSn/Ti electrodes; (c) Comparison of cyclic voltammogram of Pt/Ti with most active composition of PtPd/Ti, PtRu/Ti and PtSn/Ti electrodes in 1 M CH_3OH + 0.5 M H_2SO_4 at a scan rate of 50 mV s^{-1}.

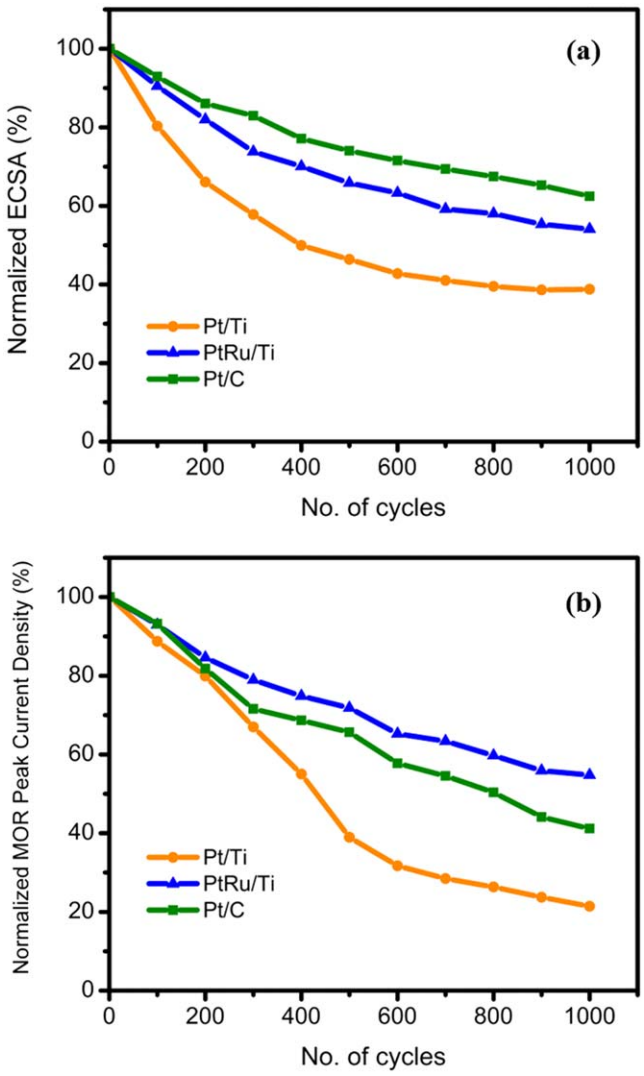

Figure 9. Comparison of (a) normalized ECSA and (b) normalized MOR peak current density measured during ADT studies for (i) Pt/C, (ii) Pt/Ti and (iii) PtRu/Ti catalysts.

PtPd and Pt. Hence, from the various compositions and binary metals prepared, PtRu/Ti with Pt to Ru ratio of 1:1 was found to be most active towards methanol oxidation. Hence, further studies were performed on the $Pt_{50}Ru_{50}$ catalyst.

Durability studies.—In order to investigate the electrocatalyst durability, accelerated durability tests (ADT) were conducted on the prepared Pt/Ti and $Pt_{50}Ru_{50}$/Ti electrocatalysts by performing continuous potential cycling between 0.6 and 1.2 V for 1000 cycles at a scan rate of 50 mV s^{-1} with periodic measurements of ECSA and MOR activity after every 100 cycles. For the purpose of comparison, ADT was also performed on commercial 40 wt.% Pt/C (Johnson Matthey) drop-casted on a glassy carbon electrode with similar loading as given in the Supporting Information.

The cyclic voltammograms of the electrodes measured in 0.5 M H_2SO_4 during ADT recorded before and after 1000 cycles are presented in Fig. S17. The ECSA for Pt/Ti dropped rapidly with respect to a number of cycles when compared to PtRu/Ti as evidenced in Fig. 9a. The ECSA for Pt/Ti decreased from 26.9 $m^2\ g^{-1}$ to 10.4 $m^2\ g^{-1}$ after 1000 cycles of ADT as opposed to a relatively lesser drop of ECSA for PtRu/Ti from 20.8 $m^2\ g^{-1}$ to 11.3 $m^2\ g^{-1}$. However, the ECSA retention for Pt/C is higher than both Pt/Ti and PtRu/Ti as the values reduced to 62%, 38%, and 54% of its initial value for Pt/C, Pt/Ti, and PtRu/Ti, respectively. This can

be due to the high surface area offered by the carbon support compared to the Ti support. Hence, we can expect that replacing Ti foil with Ti mesh or foam or nanotubular form can improve the surface area of support and thereby help reduce loss in ECSA.

The cyclic voltammograms of the electrodes measured in 0.5 M H_2SO_4 + 1 M CH_3OH during ADT recorded before and after 1000 cycles are presented in Fig. S18. As evidenced by the normalized MOR peak current density measured during ADT studies shown in Fig. 9b, the drop in catalytic performance was akin to the loss in ECSA. It is observed that the catalytic activity for Pt/Ti electrocatalyst drops by 78% after 1000 cycles as opposed to ∼45% drop for $Pt_{50}Ru_{50}$/Ti. This shows that the drop in catalytic activity is directly related to the loss in Pt atoms through Ostwald ripening, coalescence, and leaching away of oxidized Pt nanoparticles into the electrolyte.[56]

However, it is observed that PtRu/Ti showed relatively less loss in catalytic performance, suggesting enhanced stability in relation to Pt/Ti and commercial Pt/C catalyst. The increased performance and stability of PtRu/Ti electrocatalyst in comparison to Pt counterpart is attributed to the synergetic effect of the bimetallic catalyst and the stable Ti substrate, leading to the retention of ECSA and MOR peak current. In general, the Ti substrate as such is known for its higher interaction with the noble metal particles, leading to SMSI.[57] Hence, among the various bimetallic catalysts investigated, PtRu electrodeposited on Ti has higher catalytic activity and better stability. As a future scope, Ti foil substrate used in the current study can be replaced with Ti foam or mesh or Ti nanotubes to further enhance the catalytic activity and stability, and to investigate the feasibility of its application in DMFC.

Conclusions

In summary, galvanostatic pulse electrodeposition was successfully applied for the preparation of Pt and bimetallic PtPd, PtSn, and PtRu catalysts on titanium support. Various compositions of the bimetallic catalysts having the same total metal loading were prepared and screened for their performance towards methanol oxidation. The results from SEM, EDX, and XRD indicate the desired composition of bimetallic catalysts was successfully electrodeposited with various morphologies of dendritic, irregular, and spherical deposits for PtPd, PtSn, and PtRu, respectively. Analysis of cyclic voltammetry measurements indicates that PtSn and PtRu showed less-defined peaks in the hydrogen ads/des region compared to the well-defined peaks in the same region for PtPd and Pt which can be attributed to the oxophilic nature of Sn and Ru. CO-stripping studies reveal lower onset potential for CO oxidation for PtRu and PtSn as opposed to PtPd and Pt, thus confirming that the presence of Ru or Sn can lower the binding energy of CO on Pt sites, thereby facilitating easy removal of CO species. Bimetallic catalysts showed enhanced catalytic activity towards methanol oxidation than Pt on the Ti support. Among the compositions studied, $Pt_{50}Pd_{50}$/Ti, $Pt_{75}Sn_{25}$/Ti, and $Pt_{50}Ru_{50}$/Ti showed higher catalytic activity indicating the synergetic effect between Pt and the second metal. $Pt_{50}Ru_{50}$/Ti showed the highest activity during methanol oxidation studies as well as good stability during chronoamperometry studies. Additionally, ADT studies further corroborate that $Pt_{50}Ru_{50}$/Ti has enhanced stability showing relatively less loss in catalytic performance up to 1000 cycles in comparison to Pt/Ti and commercial Pt/C. Hence, it can be concluded that $Pt_{50}Ru_{50}$/Ti is the best catalyst for methanol oxidation among all the bimetallics and varied composition studied. This can pave the way for developing an electrocatalyst with Ti-based support which can be an alternative to the conventional carbon.

Acknowledgments

We would like to acknowledge the financial support from the Ministry of New and Renewable Energy (MNRE), Government of India under grant No. 102/61/2009-NT.

References

1. H. Ahmad, S. K. Kamarudin, U. A. Hasran, and W. R. W. Daud, *Int. J. Hydrogen Energy*, **35**, 2160 (2010).
2. T. S. Zhao, W. W. Yang, R. Chen, and Q. X. Wu, *J. Power Sources*, **195**, 3451 (2010).
3. M. Łukaszewski and A. Czerwiński, *J. Electroanal. Chem.*, **589**, 38 (2006).
4. U. B. Demirci, *J. Power Sources*, **173**, 11 (2007).
5. Y. Xu and B. Zhang, *Chem. Soc. Rev.*, **43**, 2439 (2014).
6. S. C. S. Lai, N. P. Lebedeva, T. H. M. Housmans, and M. T. M. Koper, *Top. Catal.*, **46**, 320 (2007).
7. Y. I. Kim, D. Soundararajan, C. W. Park, S. H. Kim, J. H. Park, and J. M. Ko, *Int. J. Electrochem. Sci.*, **4**, 1548 (2009).
8. J. Maya-Cornejo, A. Garcia-Bernabé, and V. Compañ, *Int. J. Hydrogen Energy*, **43**, 872 (2018).
9. F. Maillard, G.-Q. Lu, A. Wieckowski, and U. Stimming, *J. Phys. Chem. B*, **109**, 16230 (2005).
10. B. Hasa, E. Kalamaras, E. I. Papaioannou, L. Sygellou, and A. Katsaounis, *Int. J. Hydrogen Energy*, **38**, 15395 (2013).
11. T. Maiyalagan, *Int. J. Hydrogen Energy*, **34**, 2874 (2009).
12. S. J. Yoo, T.-Y. Jeon, K. S. Kim, T.-H. Lim, and Y.-E. Sung, *Phys. Chem. Chem. Phys.*, **12**, 15240 (2010).
13. N. S. Veizaga, V. I. Rodriguez, T. A. Rocha, M. Bruno, O. A. Scelza, S. R. de Miguel, and E. R. Gonzalez, *J. Electrochem. Soc.*, **162**, F243 (2015).
14. H. B. Hassan, *J. Fuel Chem. Technol.*, **37**, 346 (2009).
15. R. Matthew Asmussen, B. D. Adams, S. Chen, B. Shah, and A. Chen, *J. Electroanal. Chem.*, **688**, 151 (2013).
16. L.-N. Zhou, X.-T. Zhang, Z.-H. Wang, S. Guo, and Y.-J. Li, *Chem. Commun.*, **52**, 12737 (2016).
17. K.-W. Park, J.-H. Choi, B.-K. Kwon, S.-A. Lee, Y.-E. Sung, H.-Y. Ha, S.-A. Hong, H. Kim, and A. Wieckowski, *J. Phys. Chem. B*, **106**, 1869 (2002).
18. H. He, P. Xiao, M. Zhou, Y. Zhang, Y. Jia, and S. Yu, *Catal. Commun.*, **16**, 140 (2011).
19. Y. Zhang, J. Li, H. Rong, X. Tong, and Z. Wang, *Langmuir*, **33**, 5991 (2017).
20. R. Zhang, W. Xia, W. Kang, R. Li, K. Qu, Y. Zhang, B. Chen, H. Wang, Y. Sun, and H. Li, *Chemistry Select*, **3**, 3615 (2018).
21. M. Jiang, B. Lim, J. Tao, P. H. C. Camargo, C. Ma, Y. Zhu, and Y. Xia, *Nanoscale*, **2**, 2406 (2010).
22. N. M. Marković, H. A. Gasteiger, P. N. Ross, X. Jiang, I. Villegas, and M. J. Weaver, *Electrochim. Acta*, **40**, 91 (1995).
23. A. Shukla, A. Aricò, K. El-Khatib, H. Kim, P. Antonucci, and V. Antonucci, *Appl. Surf. Sci.*, **137**, 20 (1999).
24. A. O. Neto, R. R. Dias, M. M. Tusi, M. Linardi, and E. V. Spinacé, *J. Power Sources*, **166**, 87 (2007).
25. M. S. Çögenli and A. B. Yurtcan, *Int. J. Hydrogen Energy*, **43**, 10698 (2018).
26. W. Zhou, *Appl. Catal. B Environ.*, **46**, 273 (2003).
27. Q. Zhang, J. Xie, J. Liang, and J. Y. Lee, *Adv. Funct. Mater.*, **19**, 1387 (2009).
28. S. Campisi, M. Schiavoni, C. Chan-Thaw, and A. Villa, *Catalysts*, **6**, 185 (2016).
29. W. Zheng, A. Suominen, and A. Tuominen, *Energy Procedia*, **28**, 78 (2012).
30. V. Muthukumar and R. Chetty, *Ionics (Kiel).*, **24**, 3937 (2018).
31. B. G. Abraham, K. K. Maniam, A. Kuniyil, and R. Chetty, *Fuel Cells*, **16**, 656 (2016).
32. F. Nasirpouri, in *Electrodeposition of Nanostructured Materials* (Springer International Publishing, Cham) (2017).
33. S. M. Ayyadurai, Y.-S. Choi, P. Ganesan, S. P. Kumaraguru, and B. N. Popov, *J. Electrochem. Soc.*, **154**, B1063 (2007).
34. D. W. Goodman, *Catalysis Letters*, **99**, 2 (2005).
35. R. Chetty, P. A. Christensen, B. T. Golding, and K. Scott, *Appl. Catal. A Gen.*, **271**, 185 (2004).
36. H. Li, J. Wang, M. Liu, H. Wang, P. Su, J. Wu, and J. Li, *Nano Res.*, **7**, 1007 (2014).
37. D. Landolt and A. Marlot, *Surf. Coatings Technol.*, **169–170**, 8 (2003).
38. N. V. Long, Y. Yang, C. Minh Thi, N. Van Minh, Y. Cao, and M. Nogami, *Nano Energy*, **2**, 636 (2013).
39. B. Du, S. A. Rabb, C. Zangmeister, and Y. Tong, *Phys. Chem. Chem. Phys.*, **11**, 8231 (2009).
40. Z.-G. Shao, F. Zhu, W.-F. Lin, P. A. Christensen, and H. Zhang, *Phys. Chem. Chem. Phys.*, **8**, 2720 (2006).
41. R. G. Freitas, M. C. Santos, R. T. S. Oliveira, L. O. S. Bulhões, and E. C. Pereira, *J. Power Sources*, **158**, 164 (2006).
42. V. W. S. Lam, A. Alfantazi, and E. L. Gyenge, *J. Appl. Electrochem.*, **39**, 1763 (2009).
43. B. Gollas, J. M. Elliott, and P. N. Bartlett, *Electrochim. Acta*, **45**, 3711 (2000).
44. H. Zhang, W. Zhou, Y. Du, P. Yang, and C. Wang, *Electrochem. Commun.*, **12**, 882 (2010).
45. K. K. Maniam and R. Chetty, *Fuel Cells*, **13**, 1196 (2013).
46. D. C. Papageorgopoulos, M. Keijzer, J. B. J. Veldhuis, and F. A. de Bruijn, *J. Electrochem. Soc.*, **149**, A1400 (2002).
47. F. Alcaide, G. Álvarez, P. L. Cabot, H.-J. Grande, O. Miguel, and A. Querejeta, *Int. J. Hydrogen Energy*, **36**, 4432 (2011).
48. Y. Yang, L.-M. Luo, Y.-F. Guo, Z.-X. Dai, R.-H. Zhang, C. Sun, and X.-W. Zhou, *J. Electroanal. Chem.*, **783**, 132 (2016).
49. Y. Kim, Y. W. Lee, M. Kim, and S. W. Han, *Chem.—A Eur. J.*, **20**, 7901 (2014).
50. L. Li, H. Liu, C. Qin, Z. Liang, A. Scida, S. Yue, X. Tong, R. R. Adzic, and S. S. Wong, *ACS Appl. Nano Mater.*, **1**, 1104 (2018).

51. S. Stevanović, D. Tripković, V. Tripković, D. Minić, A. Gavrilović, A. Tripković, and V. M. Jovanović, *J. Phys. Chem. C*, **118**, 278 (2014).
52. H. A. Gasteiger, *J. Electrochem. Soc.*, **141**, 1795 (1994).
53. S. Chalupczok, P. Kurzweil, H. Hartmann, and C. Schell, *Int. J. Electrochem.*, **2018**, 1 (2018).
54. C. L. Green and A. Kucernak, *J. Phys. Chem. B*, **106**, 1036 (2002).
55. G. Vijayaraghavan, L. Gao, and C. Korzeniewski, *Langmuir*, **19**, 2333 (2003).
56. J. C. Meier, C. Galeano, I. Katsounaros, A. A. Topalov, A. Kostka, F. Schüth, and K. J. J. Mayrhofer, *ACS Catal.*, **2**, 832 (2012).
57. S. Shanmugam and A. Gedanken, *J. Phys. Chem. C*, **113**, 18707 (2009).